Fatigue crack growth behaviour of A5083 series aluminium alloys and their welded joints

Gotoh, Koji
Department of Marine Systems Engineering, Faculty of Engineering, Kyushu University

Murakami, Koji
Department of Civil and Structural Engineering, Graduate School of Engineering, Kyushu University

Noda, Yasuo
Department of Civil and Structural Engineering, Graduate School of Engineering, Kyushu University

出版情報：Journal of Marine Science and Technology. 16 (6), pp.343-353, 2011-09-01. Springer Japan
バージョン：

[Revised Manuscript based on the reviewers' comments]

Title: **Fatigue Crack Growth Behaviour of A5083 Series Aluminium Alloys and their Welded Joints**

(Informative title: Fatigue Crack Growth of A5083)

Authors: Koji Gotoh[1,*], Koji Murakami[2] and Yasuo Noda[3]

[1] Department of Marine Systems Engineering, Faculty of Engineering, Kyushu University

[2] Department of Civil and Structural Engineering, Graduate School of Engineering, Kyushu University

[3] Department of Civil and Structural Engineering, Graduate School of Engineering, Kyushu University

*Corresponding author:

Koji GOTOH

744 Motooka, Nishi-ku, Fukuoka, 819-0395, Japan

Tel: +81-92-802-3457

Fax: +81-92-802-3368

E-mail: gotoh@nams.kyushu-u.ac.jp

Abstract

We investigated the difference in fatigue behaviour between the aluminium alloys A5083-O and A5083-H321 because they are used as structural components in ships and high speed craft. We obtained S-N curves for the base materials and the welded joints made of A5083-O. The relationship between the fatigue crack propagation rates and the stress intensity factor ranges ΔK, ΔK_{eff} and ΔK_{RPG} [1] was determined. Additionally, the evolution of fatigue crack growth for the base materials and the welded joints made of A5083-O was measured. We also carried out numerical simulations of fatigue crack growth for both base metals and their welded joints made of A5083-O. The difference in fatigue crack growth behaviour for each alloy and the validity of the numerical simulations of fatigue crack growth based on the RPG stress criterion [1] in the base materials and their welded joints was investigated.

Keywords: Fatigue, Aluminium alloy A5083, RPG stress, Numerical simulation of fatigue crack growth

1. Introduction

The use of aluminium alloys in the hull components of ships and high speed craft is increasing because of their light weight. The A5083 series is widely applied to hull structural components because of its good resistance to sea water. Design S-N curves for A5083-O and its welded joints for evaluation have been proposed [2]. The use of A5083-H321, which is made by a different manufacturing process than A5083-O, is desirable in hull components because A5083-H321 is stronger than A5083-O. It is expected that the application of A5083-H321 will result in a reduction in hull weight. However, little information is available about the fatigue behaviour of A5083-H321 and a quantitative comparison between the fatigue behaviour of A5083-O and A5083-H321 has not been reported as far as we know.

The conventional design of hull components considering fatigue is carried out by applying the cumulative damages laws, i.e. the modified Miner's rule using the design S-N curves as specified by many design codes. Although this procedure is useful from a practical point of view it does have a serious problem in that it is not clear how transferable the fatigue life is between specimens and in-service large structures when the above-mentioned conventional procedure is applied to fatigue life estimation [3].

On the other hand, the fracture mechanics approach for the estimation of fatigue crack growth has been applied when the evolution of crack length during an operation was investigated. Fatigue crack growth histories can be estimated by applying the fatigue crack propagation laws, e.g. Paris' law or Elber's law. However, these conventional propagation laws cannot be used to evaluate various transient phenomena quantitatively, such as the retardation and acceleration of crack propagation because of an insufficient consideration of fatigue crack opening/closing caused by crack wake forming over crack surfaces. Toyosada et al. [1] proposed an improved effective stress intensity factor range based on a re-tensile Plastic Zone Generation (RPG) load, which represents the fatigue crack driving force, and developed the numerical simulation code, FLARP, to simulate the precise behaviour of a fatigue crack considering the contribution of crack wake forming to fatigue crack growth. The usefulness of their proposed method for the fatigue crack growth of steels and its welded joints has been validated [1, 4, 5]. It is expected that the application of this improved fracture

mechanics approach will become common for the fatigue life evaluation of welded structures.

To clarify the difference in fatigue behaviour of the representative aluminium alloy A5083 series and to show the possibility of numerically simulating fatigue crack growth in the base materials and welded joints of the A5083 series, we undertook the following study:

1. Comparison of the S-N curves for the base materials of A5083-O and H321.
2. Comparison of fatigue crack growth for the base materials of A5083-O and H321 and a numerical simulation of fatigue crack growth for each alloy.
3. Measurements and numerical simulations of fatigue crack growth in the cruciform welded joints of A5083-O.

The numerical simulation code FLARP [1] was used in this study.

The difference in fatigue behaviour for each alloy was confirmed by experimental results and the validity of the numerical simulation of fatigue crack growth in the base metals and welded joints of the A5083 series was carried out by comparing the measured and estimated crack growth histories.

2. Fatigue performance of the base materials

2.1 Outline of the fatigue tests

The chemical composition and mechanical properties of each material used in this study are shown in Tables 1 and 2. It can be confirmed from these tables that the H321 alloy has high performance mechanical properties, although both materials have the same chemical composition. The high performance mechanical properties are derived from the quenching and tempering process during production.

2.1.1 Fatigue tests for the S-N curves

The specimen configuration used for the fatigue tests to obtain S-N curves is shown in Figure1. Hourglass-shaped specimens were used. Fatigue tests were conducted according to the JSME testing method S002 [6]. The stress ratio (R) and loading frequency was zero (the pulsating stress condition) and 30 Hz, respectively. The rise in temperature for the

specimens was checked during the tests and it was confirmed that the rise in temperature was less than 5°C during these experiments.

2.1.2 Fatigue tests for the crack propagation rate

The specimen configuration for the fatigue crack propagation test is shown in Figure 2. Centre cracked tensile (CCT) specimens were used. We used the automation fatigue crack propagation test system developed by Toyosada et al. [4], which measures the plastic hysteresis rope consumed around a fatigue crack tip automatically and identifies the RPG and the crack opening loads from the measured hysteresis rope. Specimen compliance was measured to determine the crack length. The loading conditions for each test are shown in Table 3. Two types of loading pattern were applied. One is a constant stress amplitude pattern and the other is a decreasing stress amplitude test as regulated by the ASTM standard E-647 [5]. This was the ΔK_{th} test. Specimens O3 and H4 were subjected to the ΔK_{th} test. The maximum and minimum loads shown in Table 3 are the initial conditions. Both loads were changed according to ASTM-E647. The loading frequencies in the fatigue crack propagation tests were set to 10 Hz. The increase in specimen temperature was checked during the tests and we confirmed that the increase was less than 5 °C during the experiments.

2.2 S-N curves

S-N curves of both materials obtained by the fatigue tests are shown in Figure 3. A comparison of both S-N curves gives the results listed below:

1) The fatigue limits of both materials show a significant difference. The fatigue limit of A5083-H321 is larger than that of A5083-O. The fatigue limit ratio for both materials is approximately proportional to the yield strength ratio for both materials.

2) The fatigue strength at less than 5×10^5 cycles shows no differences for either alloy, although the yield and tensile strengths of A5083-H321 are larger than that of alloy A5083-O.

The fatigue limit of both materials is large compared to the yield and the tensile strengths of these alloys. The Aluminium

Association indicated that the ratio of fatigue strength to tensile strength for A5083-H321 is 0.508 [7]. The ratio for the same alloy obtained from Figure 3 was 0.643. No general information for A5083-O is available from the Aluminium Association. The production of a round bar type specimen and a smooth surface treatment for specimens might lead to high fatigue limits for both materials.

2.3 Fatigue crack propagation behaviour of the base materials

The fatigue crack propagation rate for each material is shown in Figure 4 (a) as a function of the stress intensity factor range (ΔK), in Figure 4 (b) as a function of the effective stress intensity factor range based on the crack opening stress (ΔK_{eff}) and in Figure 4 (c) as a function of the effective stress intensity factor range based on the RPG stress (ΔK_{RPG}). From these results, we found that the fatigue crack propagation behaviour for A5083-O and A5083-H321 was approximately the same.

The material constants for fatigue crack propagation as described by the Paris type fatigue crack propagation law ($da/dN = C\Delta K^m$, C and m: material constants) are identified from the measured crack propagation rates. The obtained material constants C and m are shown in Table 4.

Fatigue crack propagation behaves differently for different materials. The relationship between the parameter calculated by the stress intensity factor range divided into Young's modulus ($\Delta K/E$) and *da/dN* gives a unique curve for different materials [8, 9]. Similar results were reported by applying the effective stress intensity factor ranges (ΔK_{eff}) [10]. Figure 5 (a), (b) and (c) shows the fatigue crack propagation rate as a function of the parameter where the stress intensity factor range is divided into Young's modulus. The mild steel data plotted in Figure 5 was obtained from Toyosoda et al.[1]. The difference in fatigue crack propagation rate for the different materials can be eliminated by applying this parameter where the effective stress intensity factor range is divided into Young's modulus $\Delta K_{eff}/E$ and $\Delta K_{RPG}/E$. This evaluation procedure is valid for the stage II region of fatigue crack propagation when $\Delta K/E$ is used as a parameter.

2.4 Numerical simulation of fatigue crack propagation

Numerical simulations of fatigue crack propagation were performed using the numerical simulation code FLARP [1] with the material constants for fatigue crack propagation law based on the RPG stress, which is shown in the last row of Table 4. FLARP can quantitatively simulate the fatigue crack opening/closing behaviour caused by plastic wake forming over crack surfaces and has been shown to give accurate crack growth predictions under various loading histories and in residual stress fields. Detailed information of the numerical simulation procedure by FLARP is introduced in Ref. [1].

Figures 6 and 7 show a comparison of the fatigue crack growth curves obtained by FLARP with measured curves. In these numerical simulations the material constants were based on the RPG criterion shown in the last row of Table 4. The real stress loading histories were applied to the ΔK_{th} test for these simulations and they are compared in Fig. 8.

The numerical simulation results obtained by FLARP agree well with the measured curves throughout the crack propagation periods even though the stress amplitude changed during loading.

3. Fatigue crack growth evaluation of the welded joints

3.1 Outline of the fatigue crack growth tests

The chemical composition and mechanical properties of the welded joints used are shown in Tables 1 and 2, respectively. Only the A5083-O alloy was used for the fatigue tests of the welded joints because we confirmed an meaningless difference in fatigue strength at less than 5×10^5 cycles for each alloy.

Non-load carrying cruciform welded joints were used as the joint configuration. The specimen configurations are shown in Figure 9. The welding and loading conditions that were applied are shown in Tables 5 and 6, respectively.

Figure 10 shows comparisons between the measured S-N curves and the design curve for the non-load carrying cruciform welded joints [2]. The design curve is acceptable when the applied stress range is lower than 100 MPa.

In these fatigue tests, fatigue crack growth was measured for specimen N1 and specimen N2. Both the ink penetration method and the beach mark method were used to measure fatigue crack shape evolution. The measured fatigue life consists of the sum of fatigue crack initiation and propagation life.

Before the fatigue crack growth numerical simulation, the distribution of the weld toe radius along the weld lines at 10 mm intervals was measured. The minimum value of the measured weld toe radius was 0.14 mm. This value was used in the model to calculate the stress distribution in the cross section of the specimens because the fatigue crack initiates in the highest stress concentration region. Figure 11 shows the calculated stress distribution results under uniform tensile loading by elastic finite element analysis and using Glinka's formula [11]. Glinka's formula was used to estimate the distribution near the weld toe.

The residual stress distribution of the specimen that was produced using the same welding process was also investigated before the fatigue tests because the residual stress affects fatigue crack growth behaviour. Figure 12 shows the welding residual stress distributions in the cross section of the base plate obtained by the inherent stress method [12].

The inherent stress method gives the residual stress distribution of the cruciform welded joints by the following equations:

$$\sigma = 1.942\sigma_Y \left[\max \left\{ f\left(z:t\right), f\left(t-z:t\right) - N/t \right\} \right] \tag{1}$$

where

$$f\left(z:t\right) = \sum_{n=0}^{\infty} \exp\left\{ -\pi \left(2.195\, z_n / B \right)^2 \right\},$$

$$z_n = \left| z + \left\{ \left(-1\right)^n \left(n + 0.5\right) - 0.5 \right\} t \right|,$$

$$B = 1.357\sqrt{0.16Q/\sigma_Y},$$

$$N = \int_0^t \max \left\{ f\left(z:t\right), f\left(t-z:t\right) \right\} dz,$$

σ_Y : Yield stress of the base material [MPa],

z: Distance from top surface of the base plate, see Figure 9, [mm]

t: Plate thickness of the base plate [mm] and

Q: Heat input per weld length [kJ/mm].

This equation is valid when the same heat input is used for both the front and back surfaces.

Figure 13 shows a comparison of the measured residual stresses over the front and back surfaces of a specimen and the estimated stresses were calculated by the inherent stress method. We found that the estimated residual stress distribution in the cross section shown in Figure 12 is valid by comparison with the results shown in Figure 12.

3.2 Numerical simulation of fatigue crack growth

Numerical simulations of fatigue crack growth in a welded toe without an initial defect were performed according to Toyosada's procedure [4] using the numerical simulation code FLARP. A flow chart of this evaluation procedure [5] is shown in Figure 14.

In general, we observed that fatigue cracks usually initiate as plural surface cracks at a stress concentration site such as a fillet weld toe. These cracks coalesce as they advance and finally a single large surface crack appears. We also observed that the depth of the fatigue surface crack just after the completion of the coalescences is usually very small (around 0.5 mm). Considering the fatigue crack behaviour mentioned above a conventional method [4] to evaluate fatigue resistance of welded joints is proposed. The multiple fatigue cracks that grow near a welded toe were replaced with a hypothetical single surface crack in this conventional method. A semi-circle was used as the initial shape of the hypothetical single surface crack and its radius was the same as the average grain radius of the base materials.

The crack shape evolution of both joints should result in solid lines, as shown in Figure 15, when using the conventional method. The marks in Figure 15 correspond to the measured results.

Figure 16 shows the evolution of the stress intensity factors at the deepest point of a hypothetical surface crack that was subjected to a remote uniform loading and the residual stress caused by welding. The hypothetical single surface crack shape evolution shown in Figure 15, the stress distribution at the external loading shown in Figure 11 and the residual stress shown in Figure 12 were considered for the stress intensity factor calculations under both loading conditions.

The superposition method was used to calculate the stress intensity factor for the surface crack [4] and the results are shown in Figure 16. The results from this superposition method agree well with the results from the weight function method [13].

Equivalent distributed stresses (EDS) that influence finite cracks in an infinitely wide plate were introduced and they reproduce the change in stress intensity with crack depth for the advancing surface crack because of the applied load and the welding residual stress.

The corresponding variations in equivalent stresses are shown in Figure 17. The EDS distributions are shown in Figure 17 and the material constants for the fatigue crack propagation law using ΔK_{RPG} are shown in Table 4 as applied to the fatigue crack growth simulations. The loading histories that were used to insert the beach marks during the fatigue tests were also considered in the numerical fatigue crack growth simulations.

3.3 Comparison of the numerical simulations by FLARP with experimental measurements

Figure 18 shows a comparison between the estimated fatigue crack growth curves and the measured curves for each specimen. Fatigue crack initiation, which is defined as the time that the fatigue crack tip reaches the first grain boundary from the root of the weld toe can be identified by the applied estimation method. The estimated fatigue crack initiation times are shown in Figure 18 (a) and (b).

We confirmed that the fatigue crack growth rate of specimen N1 changes at about 4.0×10^5 cycles. We considered that crack propagation accelerated as the crack tip passed through the compressive residual stress region. A similar phenomenon was found at 3.2×10^5 cycles in specimen N2. This phenomenon is, however, very small compared to that in specimen N1 because the applied external stress range for specimen N2 is larger than that in specimen N1.

The estimated result for specimen N1 shows agreement with the measured value. The estimated fatigue crack growth in specimen N2 was faster than the measured growth. From both comparisons we found that the numerical simulations can safely estimate the fatigue crack growth history.

The faster life estimation for specimen N2 was due to insufficient information about fatigue crack shape evolution, as shown in Figure 15. The same crack shape evolution was assumed for both numerical simulations. The applied method for determining the surface crack shape evolution is based on a measured result from the corner boxing fillet joints wherein the fatigue crack initiation sites are limited. On the contrary, the cruciform welded joints used in this research have wide fatigue crack initiation sites. The procedure to set up the surface crack shape evolution for the cruciform welded joints might be modified in future.

4. Concluding remarks

Differences in the fatigue behaviour of the aluminium alloys, A5083-O and A5083-H321, were investigated by investigating their S-N curves and the relationship between fatigue crack propagation rates and stress intensity factor ranges. A numerical simulation of fatigue crack growth for both the base metals and their welded joints made of A5083-O was carried out.

The following results were obtained:

1. No significant difference in the fatigue strength over a finite amount of time was found between the alloys; however a significant difference was found for the fatigue limit between the alloys.
2. No significant difference was found in fatigue crack propagation behaviour between the alloys.
3. A numerical simulation of fatigue crack growth in the base materials can be performed using FLARP with suitable material constants for ΔK_{RPG} and based on the fatigue crack propagation law.
4. A numerical simulation procedure for fatigue crack growth from the weld toe can be performed according to the conventional procedure given in Ref. [4] using FLARP.

A precise investigation into the fatigue crack shape evolution for many types of welded joints is required to increase the accuracy of fatigue crack growth estimations.

Acknowledgements

This paper owes much to the thoughtful and helpful support of Mr. Tsutomu Takimoto and Mr. Keiji Akiduki (Mitsubishi heavy industries Co. Ltd., Japan). Dr. Masahiro Toyosada (Prof. Emeritus at Kyushu Univerisity) and Dr. Toshio Niwa, (Materials Reliability Group, National Maritime Research Institute, Japan) contributed to the development of the FLARP numerical simulation code.

References

[1] Toyosada, M., Gotoh, K. and Niwa,T. (2004), Fatigue crack propagation for a through thickness crack: a crack propagation law considering cyclic plasticity near the crack tip, International Journal of Fatigue, Vol.26, No.9, pp.983-992

[2] Maddox, S.J. (1982), Aluminium weldments, *Proceedings of the second International Conference on Aluminium Weldments*, III-4, Munich, ISBN 3-87017-157-X, 978-3-87017-157-5

[3] Schütz, W. (1996), A HISTORY OF FATIGUE. Engineering Fracture Mechanics, Vol.54, No.2, pp.263-300

[4] Toyosada, M., Gotoh, K. and Niwa,T. (2004), Fatigue life assessment for welded structure without initial defects; an algorithm for predicting fatigue crack growth from a sound site. International Journal of Fatigue, Vol.26, No.9, pp.993-1002

[5] Nagata, Y., Gotoh, K. and Toyosada, M., (2009), Numerical Simulations of Fatigue Crack Initiation and Propagation Based on Re-tensile Plastic Zone Generating (RPG) Load Criterion for In-plane Gusset Welded Joints, Journal of Marine Science and Technology, Vol.14, No.1, pp.104-114

[6] The Japan Society of Mechanical Engineers, Standard Method of Statistical Fatigue Testing (JSME S 002), 1994

[7] The Aluminum Association (1998), Aluminum standards and data.

[8] Speidel, M.O. (1973), STRESS CORROSION CRACKING AND CORROSION FATIGUE OF AN AUSTENITIC Ni-Cr-Fe ALLOY IN A CAUSTIC ENVIRONMENT, Institute of Metallurgy (London) Monograph Rep. Series, Vol.1, Issue 3, pp.477-481.

[9] Usami, S. (1982), Applications of Threshold Cyclic-Plastic-Zone-Size Criterion to Some Fatigue Limit Problems, Fatigue Thresholds, Warley Engineering Materials Advisory Services, pp.205-238.

[10] Jono, M, Song,J.H., Mikami, S. and Ogaki, Fatigue Crack Growth and Crack Closure Behavior of Structural Materials, M.Journal of The Society of Materials Science, Japan, Vo.33, No.367, pp.468-474 (in Japanese).

[11] Glinka, G. (1985), Calculation of Inelastic Notch-Tip Strain-Stress Histories under Cyclic Loading. Engineering Fracture Mechanics, Vol.22, No.5, pp.839-864.

[12] Matsuoka, K. and Yoshii, T. (1998), Weld Residual Stress in Corner Boxing Joints, Class NK TECHNICAL BULLETIN, Vol.16, pp.1-10.

[13] Shiratori, M., Miyoshi T. and Tanigawa K. (1986), Analysis of Stress Intensity Factors for Surface Cracks Subjected to Arbitrarily Distributed Surface Stresses, Journal of Mechanical Engineering of Japan, Vol. A52, No.474, pp.390-398 (in Japanese).

Table 1 Chemical composition of the aluminium alloys A5038-O and A5083-H321 (wt%)

Alloy type	Si	Fe	Cu	Mn	Mg	Cr	Zn	Ti
O	0.16	0.19	0.01	0.67	4.61	0.10	0.01	0.02
H321	0.16	0.19	0.01	0.67	4.61	0.10	0.01	0.02

Table 2 Mechanical properties of the aluminium alloys A5038-O and A5083-H321

Alloy type	Yield strength [MPa]	Tensile strength [MPa]	Elongation [%]
O	183	335	15.5
H321	256	367	11.2

Table 3 Loading conditions for the fatigue crack propagation test

Specimen ID	Maximum load [kN]	Minimum load [kN]	Stress ratio (R)
O1	4.06	0.240	0.06
O2	7.89	3.90	0.50
O3 *	4.19	0.243	0.06
H1	10.8	5.09	0.47
H2	8.07	2.36	0.29
H3	5.93	0.200	0.03
H4 *	6.48	0.343	0.05

*Specimens O3 and H4 were applied to the stress amplitude decreasing test (ΔK_{th}). The maximum and minimum loads listed in Table 3 are initial conditions. Both loads were changed according to ASTM-E647.

Table 4 Material constants for Paris law type fatigue crack propagation.

Fatigue crack propagation laws	C	m
$da/dN = C(\Delta K)^m$	1.46 x 10^{-11}	4.00
$da/dN = C(\Delta K_{eff})^m$	3.69 x 10^{-10}	2.81
$da/dN = C(\Delta K_{RPG})^m$	8.73 x 10^{-10}	2.51

The unit for stress intensity factor range is MPa $m^{1/2}$ and for the crack propagation rate *da/dN*, it is m/cycle.

Table 5 Welding conditions for the built-up specimen

Welding method	MIG welding
Torch travel speed [mm/s]	13.3
Voltage [V]	7.20
Current [A]	730

Table 6 Loading conditions of the fatigue test for welded joints

Specimen ID	Maximum load [kN]	Minimum load [kN]	Stress ratio (R)	(Note)
N1	94.1	47.1	0.5	Crack growth measurement
N2	61.9	3.10	0.05	Crack growth measurement
N3	112	5.60	0.05	
N4	80.2	16.0	0.2	
N5	83.9	25.2	0.3	

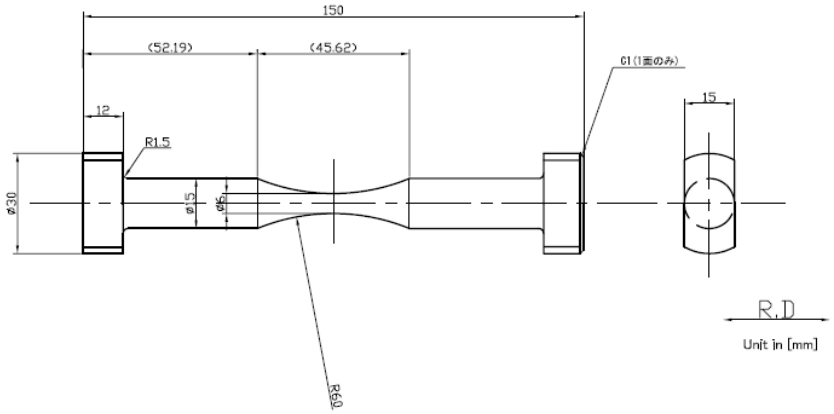

Fig. 1 Hourglass-shaped round bar specimen used in the fatigue tests.

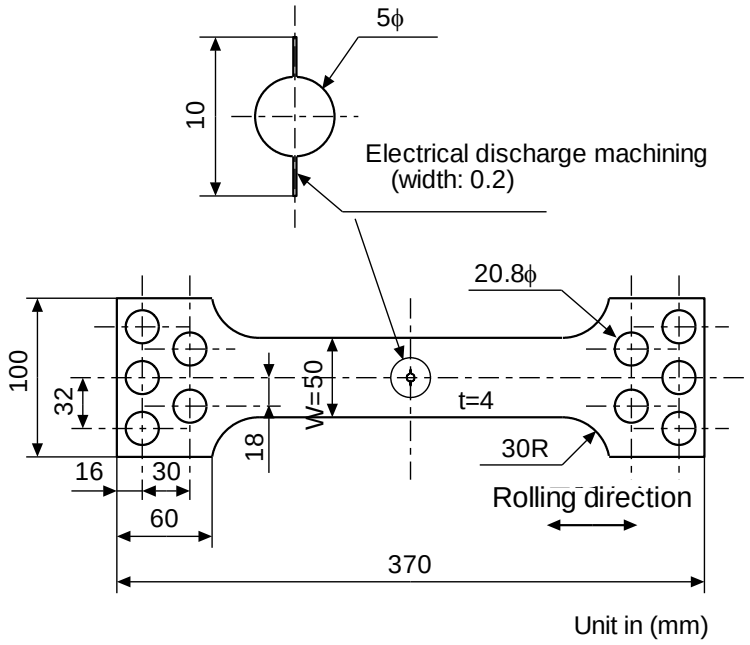

Fig. 2 Centre cracked tensile (CCT) specimen used in the fatigue crack propagation tests.

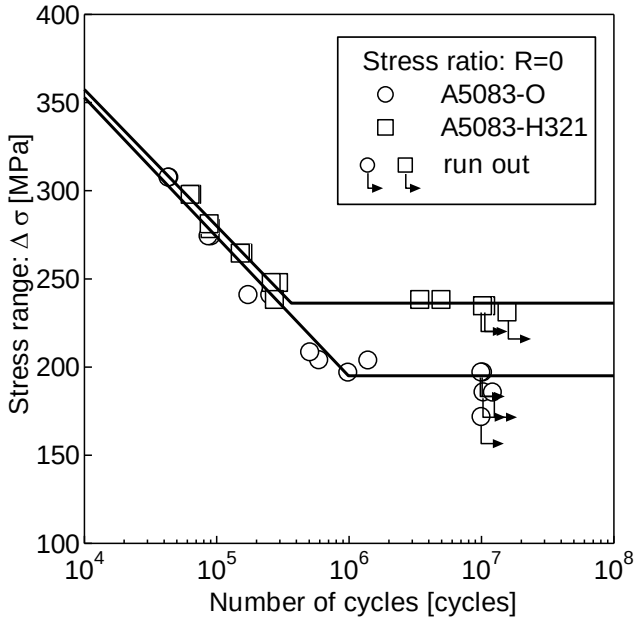

Fig. 3 S-N curves.

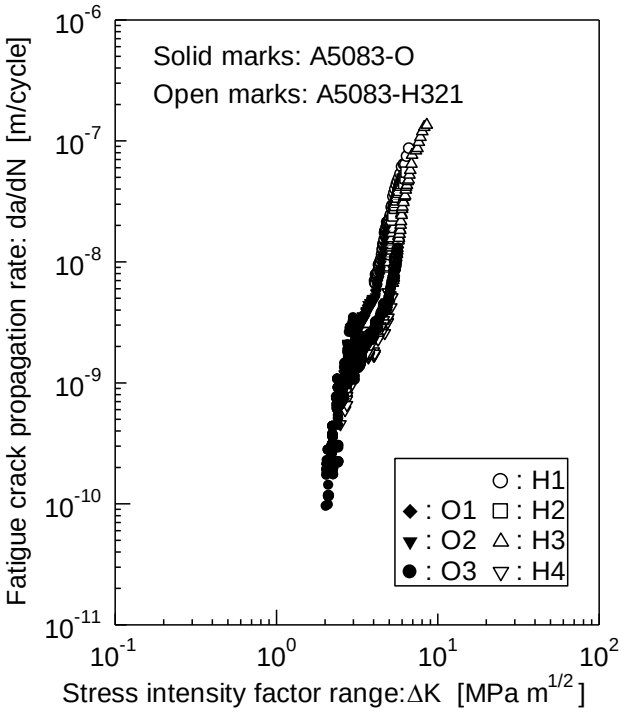

(a) $\Delta K - da/dN$

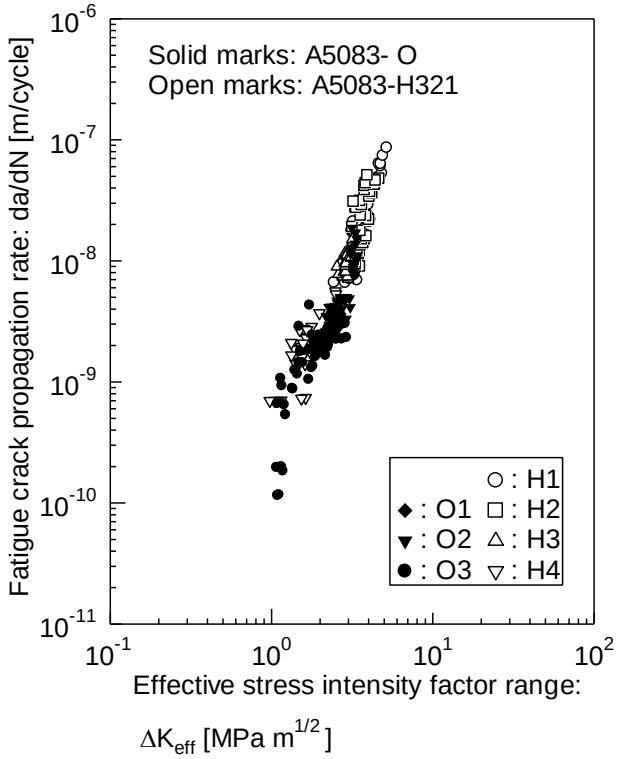

(b) $\Delta K_{eff} - da/dN$

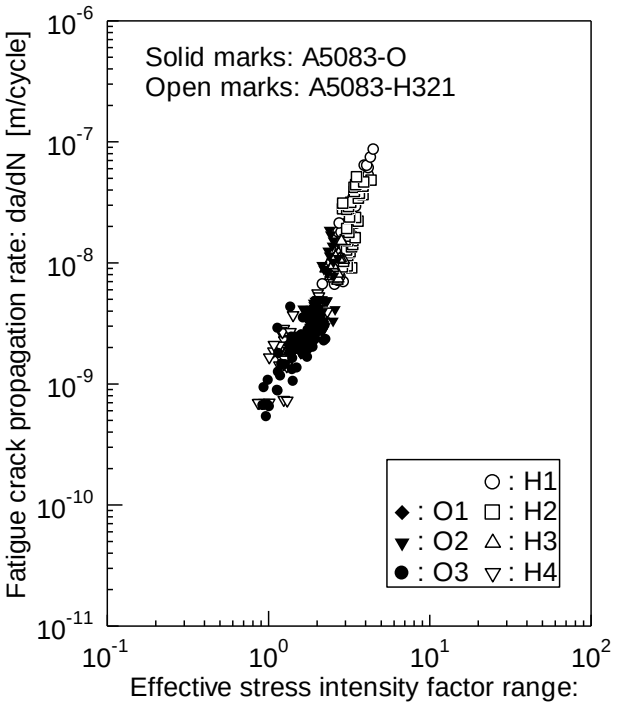

(c) $\Delta K_{RPG} - da/dN$

Fig. 4 Relationship between stress intensity factor ranges and fatigue crack propagation rate for the A5083-O and A5083-H321 materials.

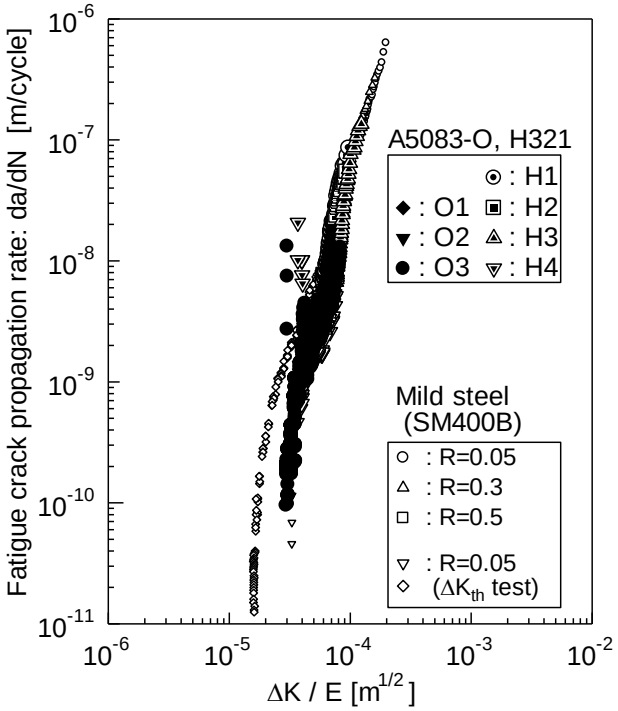

(a) $\Delta K/E - da/dN$

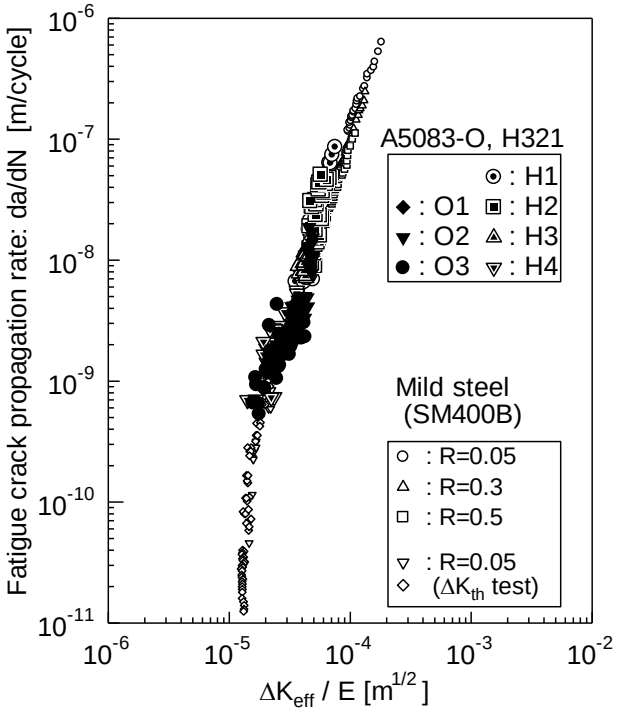

(b) $\Delta K_{eff}/E - da/dN$

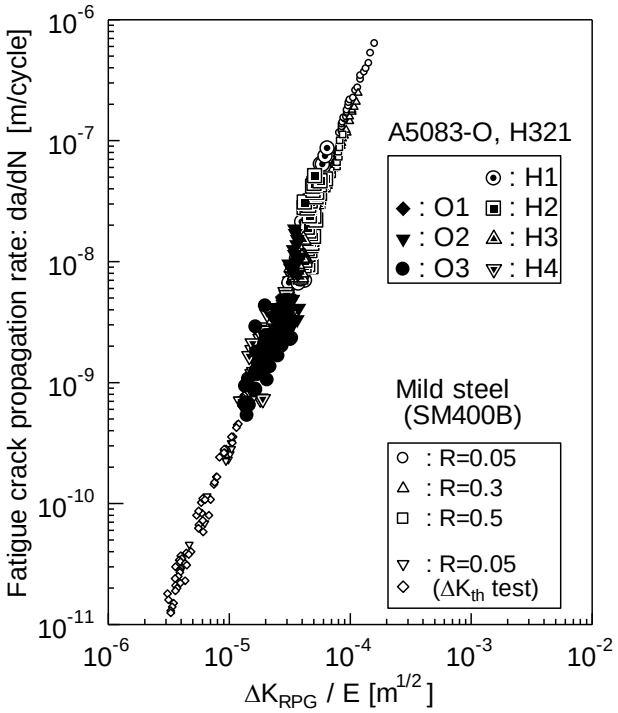

(c) $\Delta K_{RPG}/E - da/dN$

Fig. 5 Relationship between $\Delta K/E$, $\Delta K_{eff}/E$ and $\Delta K_{RPG}/E$ as well as the fatigue crack propagation rate for the A5083-O and A5083-H321 materials.

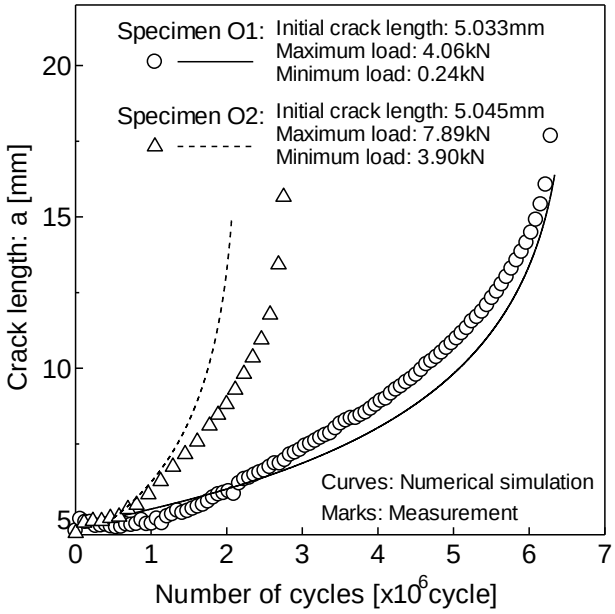

Fig. 6 Comparison of the fatigue crack growth curves obtained by FLARP and experimentally (A5083-O, constant amplitude loading).

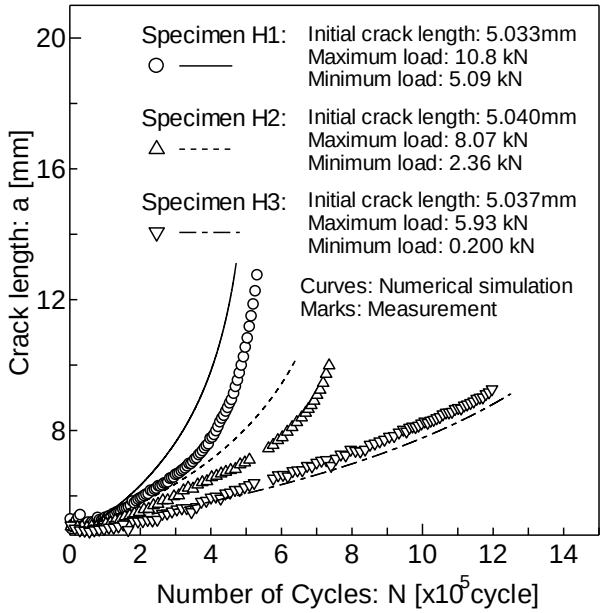

Fig. 7 Comparison of the fatigue crack growth curves obtained by FLARP and experimentally (A5083-H321, constant amplitude loading).

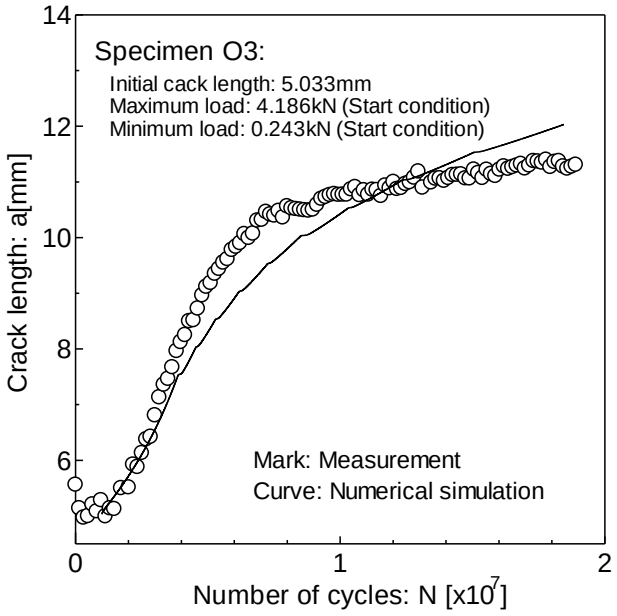

(a) A5083-O

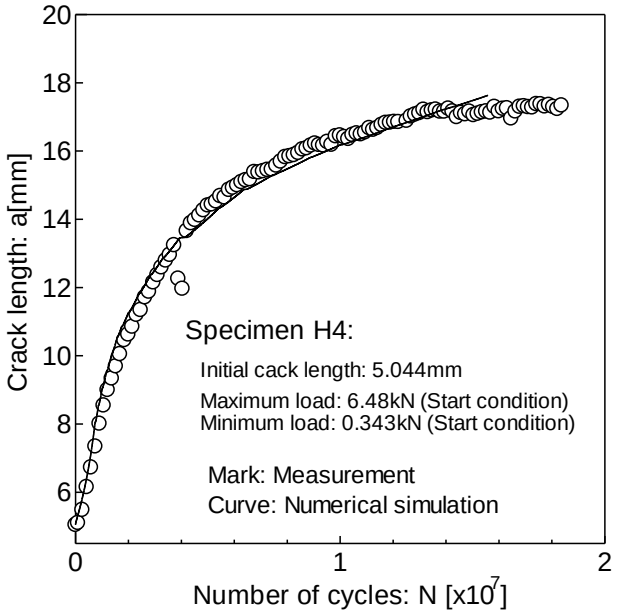

(b) A5083-H321

Fig. 8 Comparison of the fatigue crack growth curves obtained by FLARP and experimentally (ΔK_{th} tests).

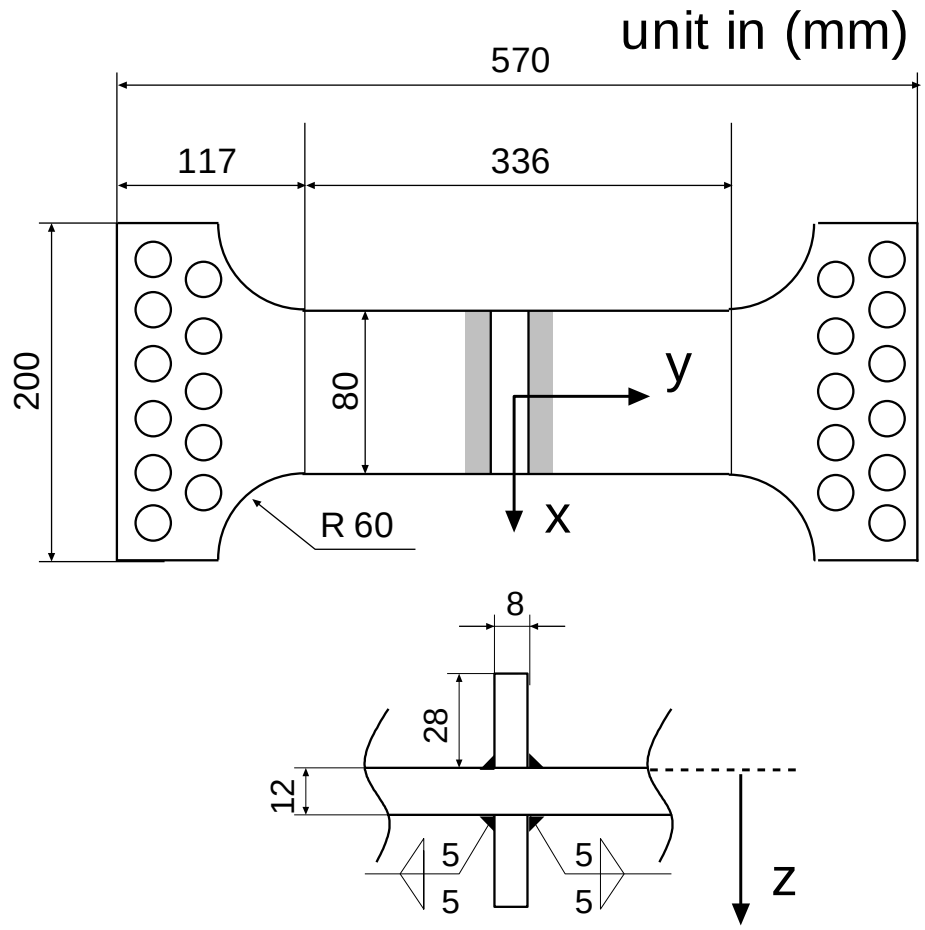

Fig. 9 Specimen configuration of the welded joints.

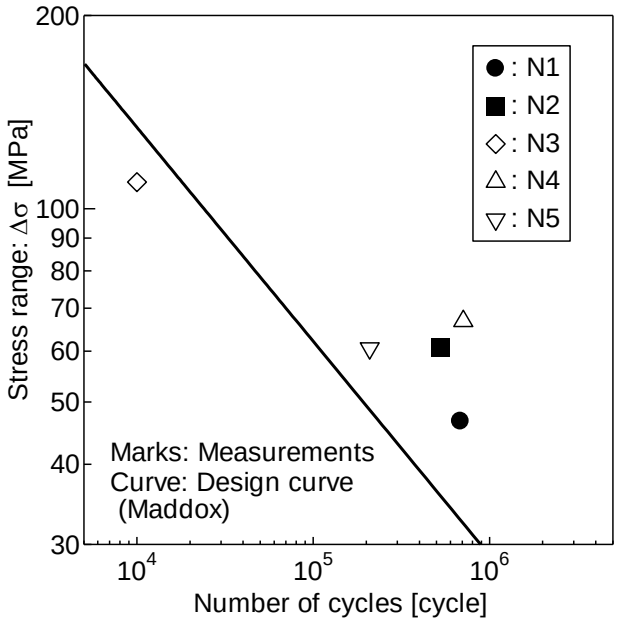

Fig. 10 Comparison of the S-N curves from the fatigue tests with a design curve by Maddox.

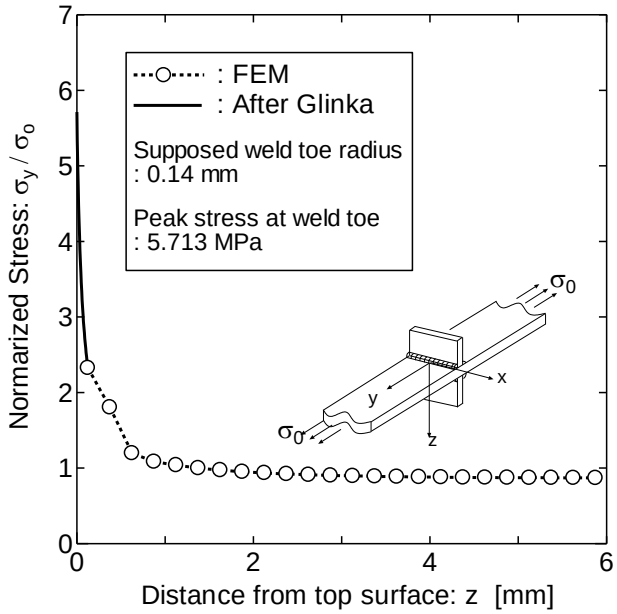

Fig. 11 Stress distribution in the cross section (y component along the z axis, x = 0).

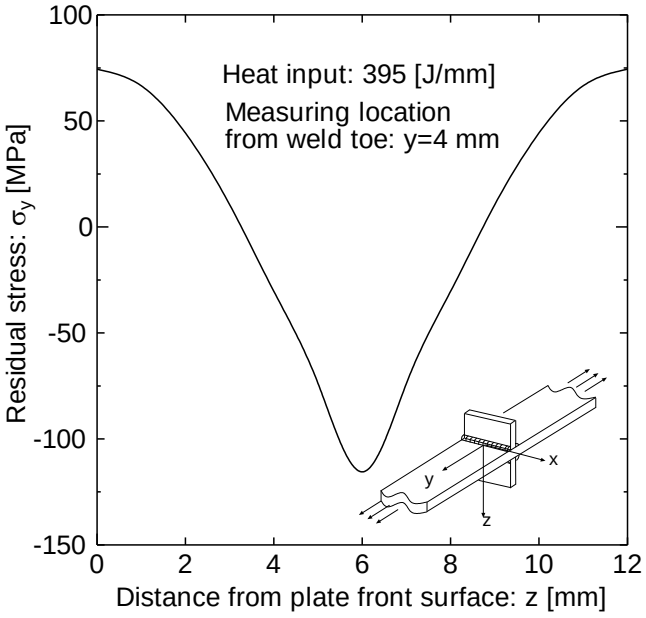

Fig. 12 Estimated residual stress distribution in the cross section of the base plate obtained by the inherent stress method.

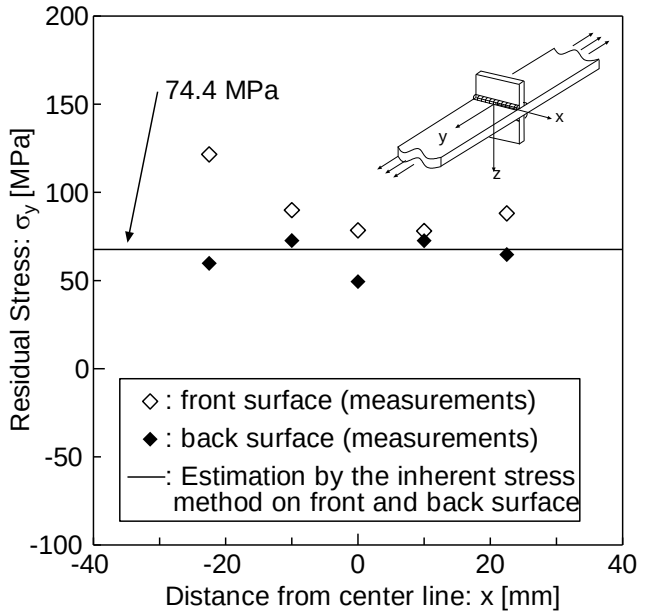

Fig. 13 Comparison between the measured residual stresses with estimated stresses determined by the inherent stress method.

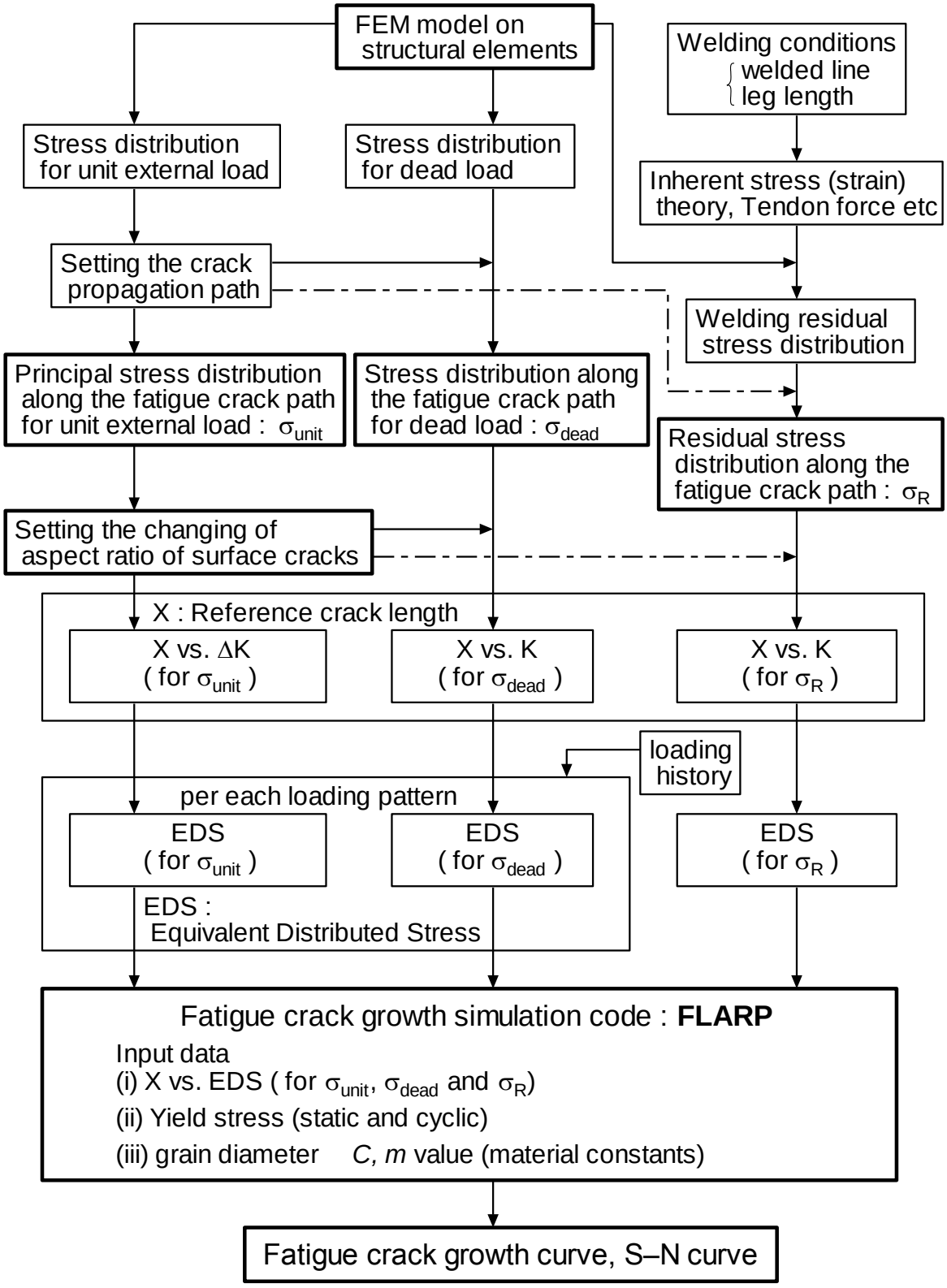

Fig. 14 Flow chart of the fatigue crack growth simulation

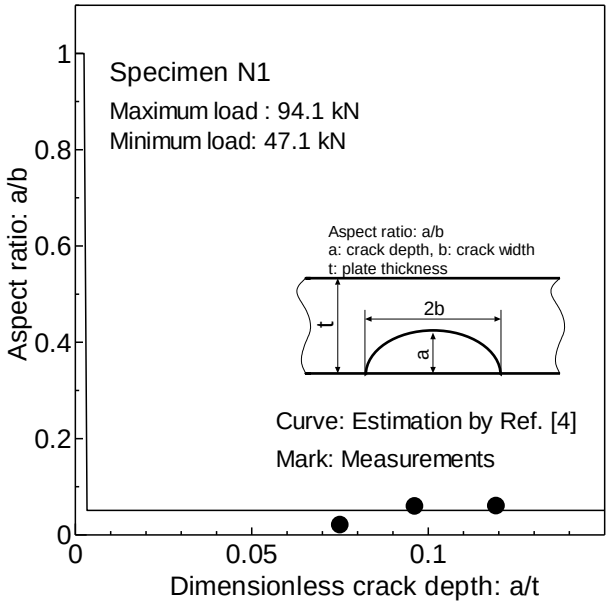

(a) Specimen N1

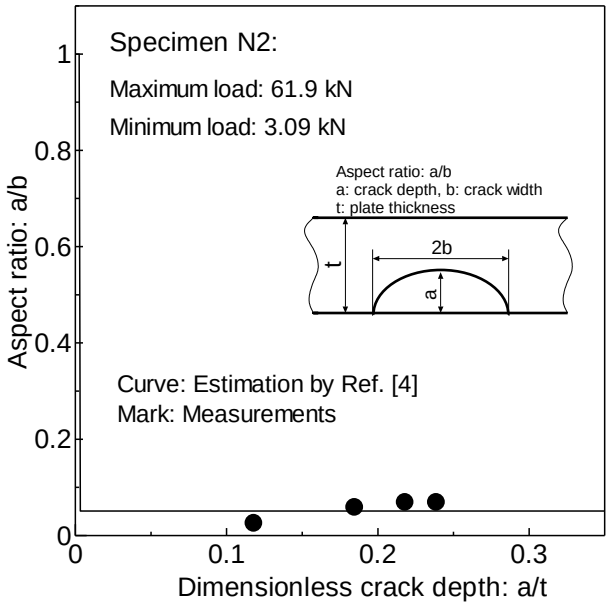

(b) Specimen N2

Fig. 15 The hypothetical surface crack evolution throughout the crack growth with measured crack shapes.

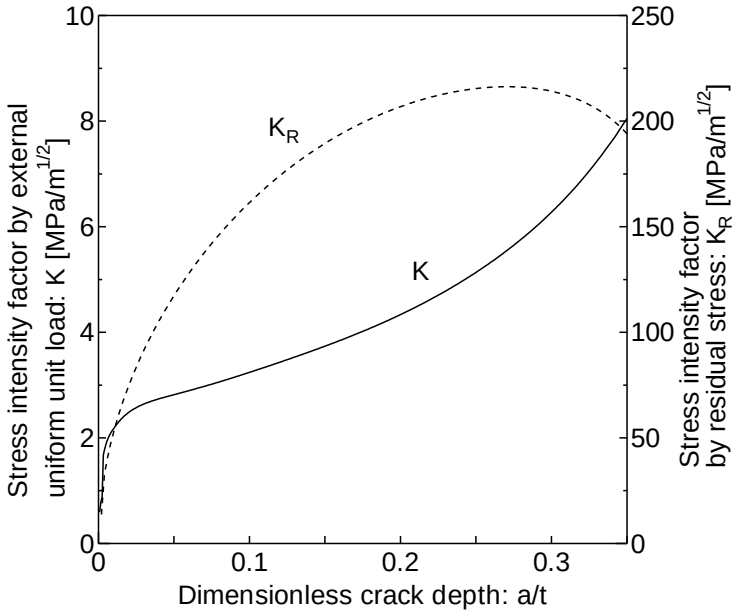

Fig. 16 Stress intensity factors as a function of crack depth.

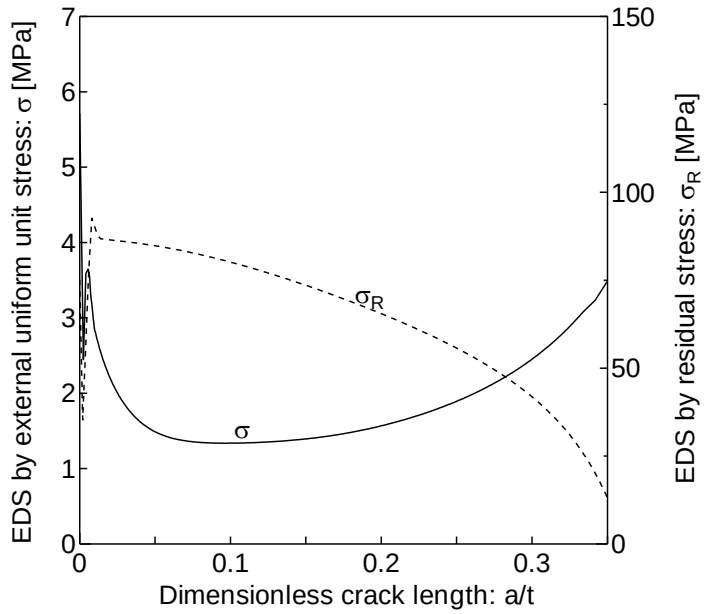

Fig. 17 Equivalent distributed stress (EDS) distribution as a function of crack depth.

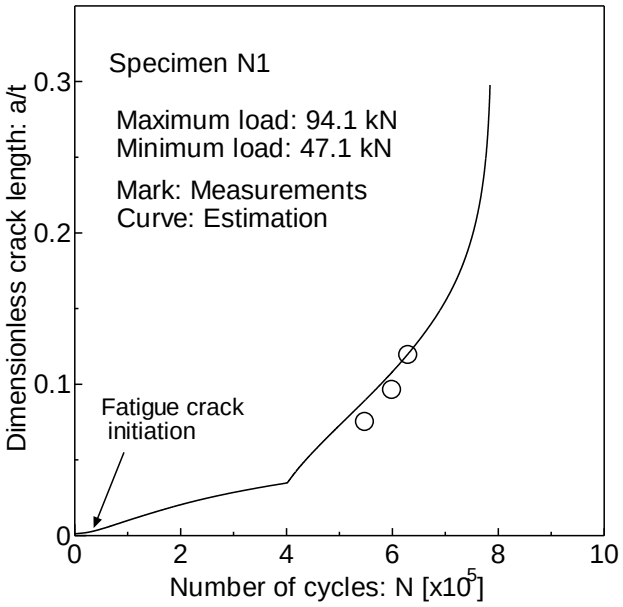

(a) Specimen N1

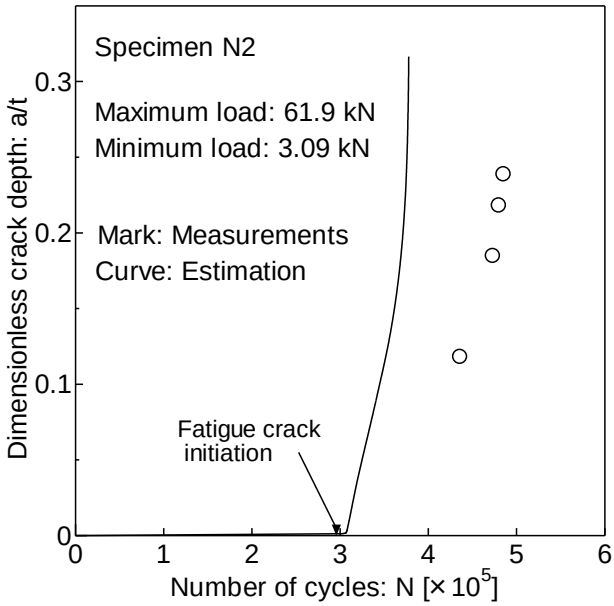

(b) Specimen N2

Fig. 18 Comparison between the estimated fatigue crack growth curves and the measured curves.